Mapping of Urban Land Surface Temperature Trends in Makassar (2000–2020) Using a Harmonic Model for Continuous Change Detection and Classification

Izzaty, A.,[1*] Hamzah, S.,[1] Wahyuni, S.,[2] Yedaya, G. I. R.,[3] Aman, M. A.[3] and Iffaty, A.[4]
[1]Civil Engineering Department, Faculty of Engineering, Universitas Hasanuddin, Gowa, South Sulawesi, 92171 Indonesia, E-mail: atikaizzaty@unhas.ac.id*
[2]Urban and Regional Planning Department, Faculty of Engineering, Universitas Hasanuddin, Gowa, South Sulawesi, 92171 Indonesia
[3]Department of Geomatics, Faculty of Engineering, National Cheng Kung University, East District, Tainan City 70101, Taiwan
[4]Urban and Regional Planning Department, Faculty of Engineering, Universitas Diponegoro, Tembalang, East Java 50275, Indonesia
Corresponding Author

DOI: https://doi.org/10.52939/ijg.v22i7.5072

Abstract
Rapid urban expansion modifies land cover, alters vegetation dynamics, and intensifies urban surface warming. This study examines long-term vegetation change, urban expansion, and land surface temperature (LST) dynamics in Makassar City, Indonesia, from 2000 to 2020 using multi-temporal Landsat imagery. Vegetation conditions were quantified using the Normalized Difference Vegetation Index (NDVI) derived from annual cloud-free composites. Temporal vegetation trajectories were analyzed using continuous change detection and classification (CCDC) based on a harmonic regression model, while urban expansion was identified through persistent vegetation loss. LST was retrieved using a consistent, sensor-specific workflow to enable interannual comparison. The results reveal a pronounced decline in vegetation between 2010 and 2015, with the strongest reductions occurring in areas where NDVI values decreased below 0.1, indicating conversion from vegetated surfaces to impervious urban land cover. During this period, urbanized areas expanded by approximately 1,500–2,000 hectares. Concurrently, mean LST increased from 22.21 °C in 2000 to 28.16 °C in 2020, representing an increase of 5.95 °C in mean urban land surface temperature (LST), primarily driven by vegetation loss and the expansion of impervious surfaces. Spatial analysis shows that the most substantial LST increases coincide with zones of sustained vegetation loss and urban expansion. These findings demonstrate the effectiveness of long-term satellite time-series analysis for detecting gradual and abrupt urban-induced environmental changes. The proposed framework provides robust evidence for monitoring vegetation degradation and urban surface warming over extended periods, offering valuable insights for urban planning and climate adaptation strategies in rapidly developing cities.

Keywords: CCDC, LST, NDVI, Spatiotemporal Analysis, Urban Sprawl

1. Introduction

The composition of the Earth's land has been significantly altered by both urban local climate change and human activities. Over the past several decades, the effects of global warming and urban-induced local climate change have become increasingly evident, particularly through the persistent rise in surface temperature. In recent studies, for example, the average surface temperature from 2000 to 2016 was 1˚C higher than the average from 1975 to 2000 [1]. Average temperatures would increase by 0.2˚C every ten years at the current rate of greenhouse gas emissions, based on the Intergovernmental Panel on Climate Change (IPCC). The increase in greenhouse gases is now conclusively connected to the observed global warming [2]. Beyond global-scale warming, increasing attention has been directed toward local and regional climate variations driven by human activities, particularly urban expansion and land surface modification. Recent studies have examined spatiotemporal urban dynamics in relation to impervious surface expansion [3] and vegetation and

ISSN: 1686-6576 (Printed) | ISSN 2673-0014 (Online)

built-up indices to detect urban sprawl based on pixel-level image analysis [4].

Local climate variability, as observed through surface temperature measurements, is closely associated with long-term urban sprawl processes. Indices such as the Normalized Difference Built-up Index (NDBI) have been widely used to assess the expansion and transformation of urban areas, especially in Makassar City, due to high urbanization [5]. Currently, the economic development in this city is the main driver of urban sprawl, which is projected to continue expanding rapidly as a key component of land use change. This expansion is largely driven by continuous development in peri-urban regions, where demand for new land leads to the conversion of previously undeveloped areas. Urban areas around the world are experiencing continuous growth in spatial extent. The transformation of rural land for urban and suburban development has become a matter of significant concern [3]. Changes in urban areas can be characterized by several features [6], including modifications to road infrastructure, ongoing construction activities, and residential development. Urban climate change is therefore manifested through higher temperatures in urban areas relative to surrounding regions [7], with land surface temperature (LST) strongly influenced by land use and land cover (LULC) properties [8] and [9]. Therefore, it is crucial to examine the connection between LULC and land surface temperature (LST) in order to understand these impacts. Global local climate change has caused an increase in LST, which has an impact on water supplies [10] and [11], vegetation, land use, and land cover [12].

Vegetation is one of the most directly detectable indicators of land surface change. The Normalized Difference Vegetation Index (NDVI) is widely used to quantify vegetation coverage and condition, making it a key indicator for monitoring urban land transformation. Land use changes and urbanization significantly influence NDVI values, primarily due to their role in elevating surface temperatures. The conversion of vegetated land into built-up areas reduces canopy cover and alters surface energy balance, intensifying temperature increases and urban heat effects [13] and [14]. Numerous studies, particularly in the United States, have investigated the relationship between NDVI and LST and characterized urban sprawl using NDBI, often through seasonal or multi-temporal image analysis [15] and [16]. The existence of vegetation on a given area of land is inherently influenced by surrounding environmental factors that contribute to temperature fluctuations. The reduction or absence of vegetation enhances the detectability of urban structures and facilitates clearer observation of spatial patterns in land surface temperature [17] and [18].

In rapidly growing Indonesian cities such as Makassar, monitoring long-term vegetation dynamics remains challenging due to persistent cloud cover and rapid land conversion. Despite extensive research on urban expansion and vegetation dynamics, most previous studies in Indonesian cities, including Makassar, rely on discrete-time change detection or post-classification comparisons, leaving long-term continuous vegetation dynamics insufficiently explored. Continuous Change Detection and Classification (CCDC) [19] provides a time-series-based approach that models long-term spectral behaviour using harmonic regression, enabling the detection of both abrupt and gradual land surface changes while accounting for seasonal variability. Unlike traditional post-classification methods, CCDC exploits the full temporal depth of Landsat observations, reducing noise from cloud contamination and allowing consistent monitoring of vegetation trajectories over long time spans. This research utilizes data from Landsat 5 TM+, Landsat 7 ETM+, and Landsat 8 OLI/TIRS sensors, which provide consistent spatial and temporal coverage for monitoring changes in vegetation and the expansion of urban areas. Focusing on Makassar City, this research applies CCDC-based vegetation change segmentation in conjunction with land surface temperature analysis over a 20-year period to examine urban sprawl dynamics in a rapidly developing tropical coastal city. To the authors' knowledge, no previous study has integrated continuous harmonic time-series modeling with urban vegetation and LST analysis in Makassar. Therefore, this study aims to evaluate long-term vegetation density changes as indicators of urban expansion and to assess their relationship with surface temperature using a continuous change detection framework.

2.Materials and Methods

2.1 Study Location

The research area is situated in Makassar City, South Sulawesi Province, on the southwest coast of Sulawesi Island. The city's coordinates are approximately 119º24′17.38″ East longitude and 5º8′6.19″ South latitude (Figure 1). Along with Medan, Jakarta, and Surabaya, Makassar City is one of Indonesia's major growth hubs, experiencing rapid urban expansion fuelled by infrastructure and development growth.

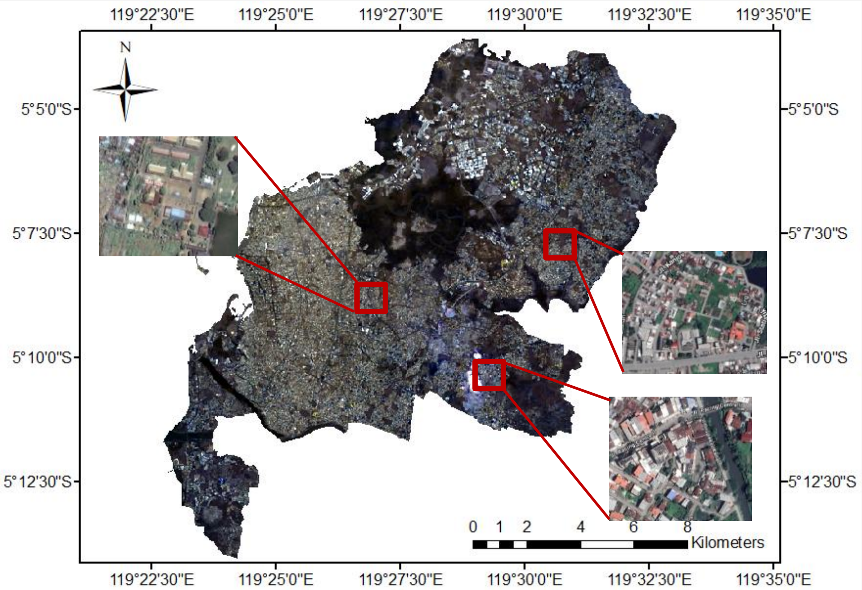

Figure 1: Makassar City, South Sulawesi, Indonesia

The topography of Makassar includes undulating land with slopes ranging from 3 to 15%, as well as flat terrain with slopes between 0 and 2%. Hilly areas are common in the eastern part of the city, while the western and northern regions are generally flatter. The typical temperatures in Makassar range from 26°C to 29°C.

Makassar City has undergone significant physical growth, with urban expansion mainly happening toward the eastern part of the city. The ongoing development of residential areas in Biringkanaya, Tamalanrea, Manggala, Panakkukang, and Rappocini districts shows this pattern of expansion. This continued outward growth is linked to the transformation of vegetated and undeveloped land into built-up areas, making Makassar City an ideal case study for examining long-term urban sprawl and vegetation changes through satellite-based time-series methods.

2.2 Data Collection

The main satellite imagery used in this research study was obtained from the Landsat program. Landsat 5 TM, Landsat 7 ETM+, and Landsat 8 OLI/TIRS imagery were used for long-term analysis covering the period from 2000 to 2020 [3]. The year 2020 was selected as the final year of analysis to ensure temporal consistency across sensors and to avoid data gaps and quality degradation associated with Landsat 7 ETM+ scan line corrector (SLC) failure and incomplete post-2020 data availability at the time of analysis. The Landsat imagery, with a spatial resolution of 30 meters, was suitable for detecting vegetation changes, urban expansion, and land surface temperature (LST). Using a spatial resolution of 30 meters, the imagery clearly captured changes over time, with cloud cover constrained to less than 10% [20]. All images were composited to produce a representative annual image for each year of observation. The data are as listed in the Table 1, with the raw images used in this study.

Satellite imagery data were processed for vegetation and land surface temperature analysis across a 20-year observation period. Changes in vegetation were analyzed using the Continuous Change Detection and Classification (CCDC) approach, which applies temporal segmentation to detect land surface changes. In this study, the Normalized Difference Vegetation Index (NDVI) was used as the primary indicator of vegetation. The CCDC algorithm, developed by [19], calculates changes at the pixel level within the defined boundaries of the study area. The algorithm is compatible with multitemporal satellite imagery, including optical data, as it models long-term spectral behaviour rather than relying on discrete classifications. The temporal segmentation process began by fitting a third-order harmonic model to each spectral band within the initial segment of the time series. Observed spectral values were compared against the model values, and a break was identified when a consistent and statistically significant deviation occurred. Following breakpoint detection, subsequent observations were assigned to a new segment until another break was detected.

ISSN: 1686-6576 (Printed) | ISSN 2673-0014 (Online) | © Geoinformatics International

Table 1: Raw images of Landsat satellite imagery

Data	Sensor	Time of Acquisition	Spatial Resolution (m)	Raw Data of Images	Spatial Reference
Landsat 5	Thematic Mapper (TM)	2000-2010	30	ee.ImageCollection("LANDSAT/LT05/C02/T1_L2")	
Landsat 7	Enhanced Thematic Mapper (ETM+)	2011-2013	30	ee.ImageCollection("LANDSAT/LE07/C02/T1_L2")	WGS-84 UTM Zone 50S
Landsat 8	OLI/TIRS (Operational Land Imager/ Thermal Infrared Sensor)	2014-2020	30	ee.ImageCollection("LANDSAT/LC08/C02/T1_L2")	

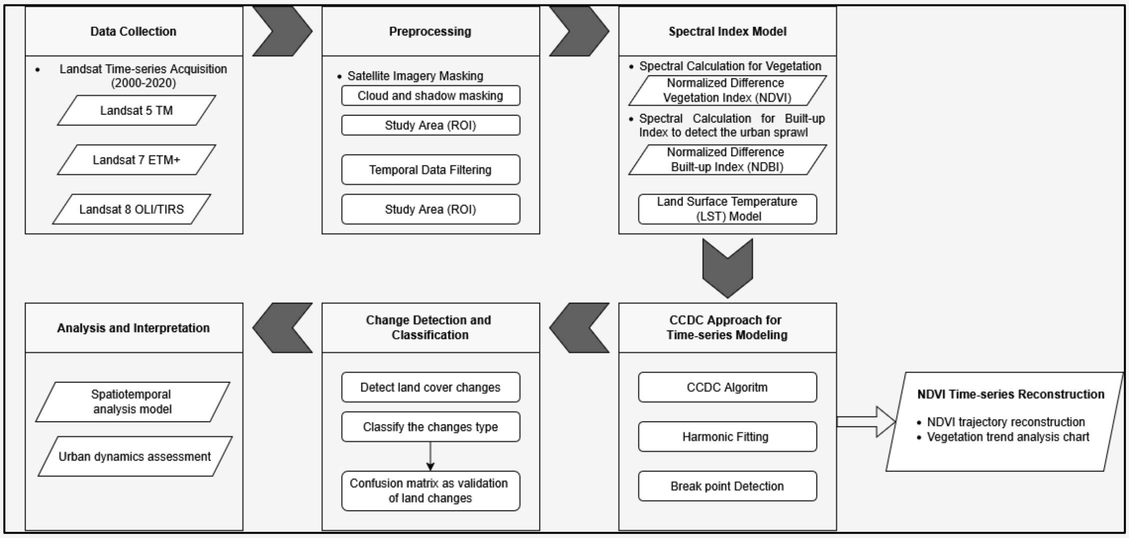

Figure 1: Land cover transformation and LST analysis using CCDC algorithm study workflow

Over the 20-year period, specific areas within Makassar City can be identified, from those that underwent early changes to those affected more recently. The final variable examined in this study was land surface temperature (LST), which served as an indicator of surface thermal conditions. Temporal variations in average surface temperature were analyzed using the thermal bands of Landsat imagery over the 20-year period.

2.3 Methods

This research shows how the prototype of the CCDC approach, with several components inside and the segmentation principle can be used in detecting the loss and gain of vegetation. Furthermore, it will evaluate the influence of climate change by analyzing temperature increases observed in the study area. The methodology is presented in Figure 2.

2.4 Preprocessing of Satellite Imagery

2.4.1 Filtering of cloud and cloud shadow

The dataset employed in this study comprises Level-2 satellite imagery, which has undergone atmospheric correction and geometric registration. Consequently, the imagery was directly utilized by applying filter masking techniques [21] to minimize cloud contamination. This initial pre-processing step was considered critical, as emphasized by [22]. Cloud masking was performed within the Google Earth Engine (GEE) environment using the quality assessment (QA) bands provided with the Landsat Collection 2 Level-2 products. Pixels flagged as cloud, cloud shadow, or cirrus in the QA_PIXEL band were excluded from further analysis. In addition, only images with overall scene-level cloud cover less than 10% were retained to reduce residual cloud contamination [20]. For each year of observation, the remaining cloud-free images were composited using a median composite approach to generate a single representative annual image.

Cloud masking is a widely implemented pre-processing technique aimed at improving image quality by reducing the presence and shadow effects of clouds [23], which in turn mitigates the risk of significant processing errors. Although such techniques do not entirely eliminate cloud-affected regions [19] and [24], they are effective in minimizing distortions associated with cloud interference.

2.4.2 The time series model of the CCDC approach

The changes of land surface are categorized as the abrupt change [19] which the vegetation driven by environmental causes the urbanization, fire, deforestation, and insects. An abrupt change is characterized as a statistically significant structural discontinuity in a pixel's modeled spectral trajectory. The algorithm first applies a harmonic regression model to represent stable seasonal patterns and inter-annual variability. A breakpoint is detected when a sequence of observed values consistently deviates from the model prediction by the segment. The changes give the break point, which is estimated by surface change coefficients in Ordinary Least Squares (OLS) on the Landsat observation images [19]. The Continuous Change Detection and Classification (CCDC) harmonic regression model used to fit the Landsat time-series observations is expressed in Equation 1[19].

$$\hat{\rho}(i,x)_{OLS} = a_{0,i} + a_{1,i}\cos\left(\frac{2\pi}{T}x\right) + b_{1,i}\sin\left(\frac{2\pi}{T}x\right) + c_{1,i}x \quad \left\{\tau^*_{k-1} < x \le \tau^*_k\right\}$$

Equation 1

Where x is the Julian date, $\hat{\rho}(i,x)_{OLS}$ is the predicted value for the ith Landsat Band at the Julian date x, for the i as the i^{th} Landsat Band, then the component $x_{0,i}$ is the overall coefficient value for the i^{th} Landsat band, $a_{1,i}$, and $b_{1,i}$ are the coefficient of intra-annual change for the *ith* Landsat band, $c_{1,i}$ is the coefficient for inter-annual change for the i^{th} Landsat band, T is the number of days in a year (T=365 days), and τ^*_k is the k^{th} break point.

The segmentation in CCDC was applied to Landsat surface reflectance bands to model continuous spectral trajectories and detect temporal breakpoints. NDVI time series were subsequently derived from the fitted reflectance values within each stable segment, allowing the reconstruction of temporally consistent vegetation dynamics.

The time series model shows a component by integrity into one trend and captures the break point changes well. Basically, this approach is based on comparing model predictions with clear satellite imagery to identify changes. In an ideal scenario, a single-date comparison would be enough to accurately detect changes. The CCDC algorithm measures the discrepancy between actual observations and model predictions for both the initial and final observations. The breakpoint detection criteria used in the CCDC algorithm are defined in Equations 2 to 4 [19].

$$\frac{1}{k}\sum_{i=1}^{k}\frac{\left|z_{1,i}(x)\right|\times t_{model}}{3RMSE_i} > 1$$

Equation 2

or

$$\frac{1}{k}\sum_{i=1}^{k}\frac{\left|\rho(i,a_1) - \hat{\rho}\right|(i,a_n)_{OLS}}{3RMSE_i} > 1$$

Equation 3

or

$$\frac{1}{k}\sum_{i=1}^{k}\frac{\left|\rho(i,a_n) - \hat{\rho}\right|(i,a_n)_{OLS}}{3RMSE_i} > 1$$

Equation 4

Where x is the Julian date as well, a_1 is the first observation during the initialization of the model in the Julian date, is a_n the last observation during initialization of mthe modelin the Julian date. For the k means the number of Landsat bands used in this research, which is 7, i is the ith Landsat band, $RMSEi$ is the value of $RMSE$ at the *ith* Landsat Band, t_{model} as the initialization model used in total time, $z1, i$ is the coefficient for inter-annual change for the ith Landsat band. Then the observed value for the ith Landsat Band at Julian date a is shown as $\rho(i,a)$ and $\hat{\rho}(i,a_n)_{OLS}$ indicate the predicted value for the ith Landsat Band at Julian date according to OLS fitting.

In the CCDC algorithm, a breakpoint is detected when the difference between the observed value and the model prediction exceeds three times the Root Mean Square Error (3RMSE) of the model residuals to identify statistically significant deviations from the fitted temporal trajectory while minimizing false detections caused by noise or seasonal variability in satellite observations [19], especially for detecting land surface changes in Landsat time-series data. To ensure transparency and reproducibility, Table 2 presents the key parameters used in the implementation of the CCDC algorithm within GEE. These parameters include the breakpoint detection settings, statistical thresholds, minimum observation requirements, and model regularization configurations applied in this study.

Table 2: List of key parameters used for CCDC approach in GEE

Parameter	Value used
Algorithm	ee.Algorithms.TemporalSegmentation.Ccdc()
Breakpoint Bands	GREEN, RED, NIR, SWIR1, SWIR2, NDVI
T-Mask Bands	GREEN, SWIR2
min Observations	6
chi-Square Probability	0.99
min Num of Years Scaler	1.33
lambda	0.005
max Iterations	10000
Scene-level Cloud Filter	CLOUD_COVER < 10%
NDVI Range	0 < NDVI < 1
Magnitude Visualization Range	-0.15 to 0.15

2.5 Long-term Detection of Urban Sprawl Area

In referencing urban expansion, a key measurable indicator closely associated with the extent of urbanization is the built-up condition. Over the past two decades, rapid development has been observed in Makassar City. To quantify this growth, particularly the expansion of built-up surfaces, in peri-urban and suburban zones, urban sprawl was detected using a built-up spectral index derived from Landsat imagery [25]. The Normalized Difference Built-up Index (NDBI) was calculated using Equation 5 [25].

$$NDBI = \frac{SWIR - NIR}{SWIR + NIR}$$

Equation 5

Because NDBI alone may misclassify certain non-urban surfaces, such as bare soil or bright impervious-like materials, urban sprawl detection was implemented using an NDBI-based thresholding approach followed by visual verification. Pixels were initially classified as built-up when NDBI values exceeded 0.3, applied consistently across all observation years. Furthermore, NDVI values lower than 0.3 were used as an additional indicator of low vegetation density, helping to distinguish built-up areas from vegetated surfaces. This combined interpretation improves the reliability of identifying urbanized land cover characterized by low vegetation and higher impervious surface reflectance. The spatial patterns of detected urban expansion were then cross-checked using high-resolution reference imagery to reduce misclassification.

2.6 Spatiotemporal Analysis of Land Surface Temperature (LST)

This radiance data then served as the basis for calculating the brightness temperature, in accordance with the method described by [14].

$$BT = \frac{K_2}{Ln\left[\frac{K_1}{L_\lambda} + 1\right]} - 273.15$$

Equation 6

The thermal calibration constants K_1 and K_2 are sensor-dependent. For Landsat 5 TM, K_1 is 607.76, and K_2 is 1260.56; for Landsat 7 ETM+, K_1 is 666.09, and K_2 is 1282.71; and for Landsat 8 TIRS Band 10, K_1 is 774.8853 and K_2 is 1321.0789. The radiant temperature is then adjusted by adding absolute zero (273. 15°C) in order to get the value in degrees Celsius.

For Landsat 7 ETM+, post-2003 imagery is affected by the scan line corrector failure (SLC-off), which introduces wedge-shaped data gaps. To reduce the impact of these gaps on annual LST estimation, the analysis relied on multi-date image availability and the annual compositing strategy described in Section 2.4, which minimized missing-data influence on the yearly thermal signal. Subsequently, the calculated brightness temperature is further processed by estimating surface emissivity, which is derived using a vegetation index. The NDVI was computed using surface reflectance values from the red and near-infrared bands, ensuring consistency across sensors and acquisition dates. This calculation is essential in evaluating the current condition of vegetation and drawing conclusions about its overall health and coverage. NDVI was used to detect vegetation changes by analyzing temporal variations in vegetation greenness across the study area. To ensure consistency and minimize seasonal effects, NDVI comparisons were conducted using imagery from similar seasonal periods each year, allowing abrupt vegetation changes to be identified more reliably. The Normalized Difference Vegetation Index (NDVI) was calculated using Equation 7.

$$NDVI = \frac{NIR - RED}{NIR + RED}$$

Equation 7

The NIR band refers to the near-infrared spectral channel, while the Red band represents the spectral channel corresponding to the red portion of the visible spectrum. The proportion of vegetation is determined by analyzing vegetation index values derived from these bands within the designated study area. The vegetation fraction, which represents the average emissivity of a unit area of the Earth's surface obtained from NDVI values, is determined using the Equation 8:

$$P_v = \left(\frac{NDVI - NDVI_{\min}}{NDVI_{\max} - NDVI_{\min}} \right)^2$$

Equation 8

Surface emissivity (ε), derived from the proportion of vegetation, is crucial in modifying blackbody radiance in accordance with Planck's law and is required for accurate LST estimation. In addition, ε represents the efficiency of thermal energy transfer from the Earth's surface to the atmosphere [26]. Using the recommended approach, ground emissivity is defined in Equation 9.

$$\varepsilon_\lambda = \varepsilon_{v\lambda} P_v + \varepsilon_{s\lambda} \left(1 - P_v\right) + C_\lambda$$

Equation 9

Where, P_v denotes the proportion of vegetation, and C_λ is a surface roughness correction term assigned a constant value of 0.005. The Emissivity of vegetation and soil is represented by $\varepsilon_{v\lambda}$ and $\varepsilon_{s\lambda}$, respectively, as defined by [27]. For thermal infrared sensors, the thermal wavelength/band (λ) corresponds to the Landsat TIR band used for LST retrieval; in this study, λ refers to Band 10, which was used in the LST calculation. The final step in deriving LST, or the emissivity-corrected LST (LST_s), is carried out using the following procedure. Equation (12), adapted from [26], applies to mixed pixels containing both vegetation and bare soil. For pixels that are predominantly vegetated or predominantly bare soil, emissivity may be approximated using vegetation- or soil-specific values, respectively. However, because Makassar City exhibits heterogeneous urban and peri-urban land cover at 30-m spatial resolution, a large proportion of pixels represent mixed surface components. Therefore, we adopted the mixed-pixel emissivity formulation to ensure methodological consistency and to avoid the use of hard land-cover thresholds in emissivity assignment. Land surface temperature was derived from Equation 10.

$$T_s = \frac{BT}{1 + \left[\frac{\lambda \cdot BT}{\gamma} Ln\left(\varepsilon_\lambda\right) \right]}$$

Equation 10

Where BT refers to the brightness temperature, γ represents a constant derived from Planck's law, and ε_λ denotes surface emissivity, each of which has been derived from previous calculations. Both LST and NDVI can be used to observe spatiotemporal changes within the study area by identifying temporal variations. These observations help in understanding continuous patterns of change associated with LST and vegetation indices over the study period.

3. Results and Discussion

3.1 Urban Sprawl Detection Driving to Loss of Vegetation

The expansion of urban areas has led to noticeable land cover changes in Makassar City over the past two decades. Built-up expansion was mapped from annual Landsat composites using the NDBI-derived built-up mask described in Section 2.5. Urban areas were extracted by applying a consistent NDBI threshold across all years (to ensure comparability in time-series interpretation), followed by visual verification using high-resolution reference imagery (Google Earth) to reduce misclassification of bright bare soil and other non-urban surfaces. Figure 3 presents the spatial distribution of newly converted built-up areas by time epoch, so that changes between periods reflect real land conversion rather than visualization differences. Certain areas experienced transformation earlier than others, with newer changes emerging more recently. The results indicate a clear spatial progression of urban growth, with early expansion concentrated in the western coastal and core urban zone, followed by a stronger outward shift toward the north and east in later periods. This pattern is consistent with Makassar's coastal-city development structure, where early growth typically intensifies around the established city center and coastal economic activities, while later expansion follows the emergence of new development corridors and the availability of larger developable land parcels in peri-urban districts.

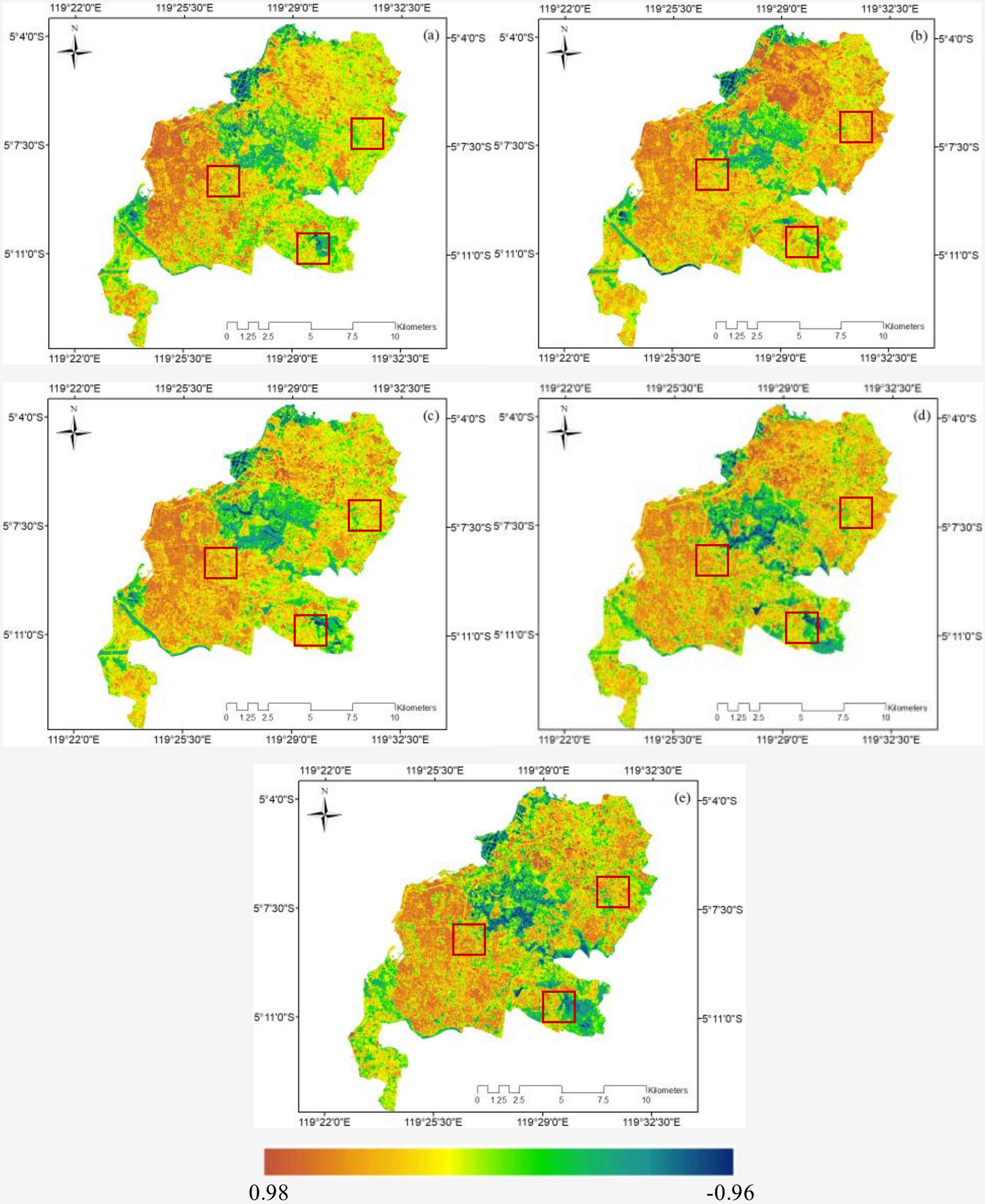

Figure 2: Transition maps of NDBI: (a) 2000, (b) 2005, (c) 2010, (d) 2015, and (d) 2020

The most pronounced acceleration occurred during 2010–2015, suggesting a period of intensified land conversion linked to major planning and development momentum. Urban growth and spatial expansion over a five-year period have led to the phenomenon of prolonged drought, driven by rising temperatures experienced by the city alongside the increase in built-up areas. Vegetation clearing, particularly the cutting of trees, has intensified, and many areas have been affected by fires. This is supported by data from the local fire department. This could be the Makassar's urban spatial planning framework for 2010–2030 (RTRW), which explicitly delineates multiple strategic development zones (including integrated port, settlement, industrial, and airport areas), which can incentivize rapid conversion of open/vegetated land when implemented through permits and infrastructure expansion.

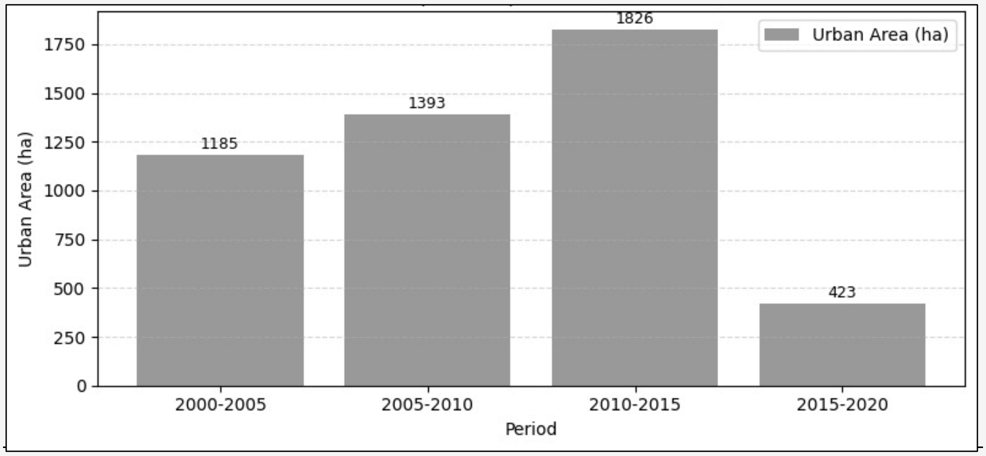

Figure 3: Distribution chart of urban sprawl between 2000-2020

Table 3: Confusion matrix for the accuracy assessment of classification changes area

2005	**Vegetation**	**Waterbody**	**Built-up**	**Bare land**	**Agriculture**	**Grassland**
Vegetation	**150**	1	3	6	0	0
Waterbody	5	**60**	0	8	3	2
Built-up	2	1	**65**	5	1	2
Bareland	2	0	6	**142**	0	2
Agriculture	3	0	0	0	**37**	1
Grassland	2	1	2	9	0	**84**
OA (%)			88.90			
Kappa Coefficient			0.84			
2010	**Vegetation**	**Waterbody**	**Built-up**	**Bare land**	**Agriculture**	**Grassland**
Vegetation	**147**	1	3	2	6	5
Waterbody	2	**62**	1	0	1	2
Built-up	2	1	**62**	3	0	1
Bareland	1	2	8	**149**	2	2
Agriculture	2	0	0	0	**40**	1
Grassland	2	1	2	9	0	**83**
OA (%)			89.75			
Kappa Coefficient			0.85			
2015	**Vegetation**	**Waterbody**	**Built-up**	**Bare land**	**Agriculture**	**Grassland**
Vegetation	**143**	1	3	1	0	0
Waterbody	0	**65**	2	0	0	0
Built-up	2	1	**79**	5	1	2
Bareland	2	0	3	**153**	6	2
Agriculture	1	0	3	0	**35**	1
Grassland	2	1	2	9	0	**80**
OA (%)			91.73			
Kappa Coefficient			0.88			
2020	**Vegetation**	**Waterbody**	**Built-up**	**Bare land**	**Agriculture**	**Grassland**
Vegetation	**140**	1	3	2	0	0
Waterbody	0	**70**	1	0	1	1
Built-up	0	1	**62**	3	0	1
Bareland	1	0	9	**155**	4	2
Agriculture	2	0	2	4	**43**	1
Grassland	2	1	2	9	0	**82**
OA (%)			91.23			
Kappa Coefficient			0.87			

The earlier dominance of development in the western coastal area can be interpreted as a continuation of growth around the historical urban core and coastal economic functions, whereas the later shift toward the north and east aligns with expansion pressures into designated settlement and airport-influenced zones identified in the RTRW planning structure. In addition, the broader infrastructure and logistics development trajectory in the Makassar region, including port-related expansion initiatives, likely increased development attractiveness and land conversion pressure during the mid-study period. The reduced rate of newly converted built-up area after 2015 may reflect a combination of factors such as (i) partial saturation of easily developable land near the earlier growth front, (ii) shifting development from extensive outward conversion to more infill or consolidation, and/or (iii) stronger constraints from land availability, permitting, or environmental limits typical of coastal cities. These interpretations should be considered alongside the year-by-year trajectory in Figure 3, which together clarify whether the slowdown reflects fewer new conversions or a redistribution of growth into different spatial forms.

This 2010–2015 acceleration is plausibly linked to the translation of Makassar's RTRW 2010 to 2030 priorities into on-the-ground development, as the plan delineates multiple Integrated Strategic Areas intended to concentrate urban functions (including coastal/port-related activities, industry, and settlement expansion), which can trigger rapid land conversion when accompanied by permitting and infrastructure [28]. The validation data were collected from high-resolution imagery available in Google Earth and were used as reference samples to assess the accuracy of the land cover classification. These reference points were visually interpreted to ensure consistency with the classified land cover categories. The confusion matrix is presented in Table 3.

3.2 Vegetation Change Detection using Harmonic Approach in Urban Area

This section reports vegetation dynamics in Makassar City during 2000–2020 based on NDVI time-series analysis using the CCDC harmonic (temporal segmentation) approach. Makassar's rapid urban growth increased pressure on peri-urban land, contributing to vegetation conversion in development corridors. To ensure comparability, NDVI was computed from Landsat surface reflectance and analyzed as a continuous time series rather than as single-date imagery. The CCDC harmonic model explicitly accounts for seasonal NDVI variability, allowing vegetation change to be interpreted from statistically significant breakpoints and sustained shifts in NDVI level, rather than from normal wet–dry seasonal cycles. Consistent with the urban sprawl patterns (Section 3.1), vegetation loss was concentrated in areas undergoing conversion to built-up land. Figure 4 shows that vegetation decline intensified in the north and east of Makassar. To support interpretation for readers unfamiliar with the study area, the location of Sultan Hasanuddin International Airport was annotated on the map.

For map-based comparison, NDVI in Figure 5 was displayed using a fixed value range across all epochs (2000, 2005, 2010, 2015, 2020), ensuring that spatial differences reflect real change rather than differences in color scaling.

Three representative sample locations (P1–P3) were selected to illustrate typical CCDC breakpoint behaviours in areas where (i) NDVI showed a sustained drop identified by CCDC and (ii) the post-break surface condition was visually confirmed as non-vegetated or built-up using high-resolution reference imagery (Figure 6).

A conversion signal is indicated when NDVI shifts to a persistently low, weakly seasonal trajectory after the breakpoint, consistent with vegetation removal and subsequent built-up or bare-surface dominance. Sample point P3 experienced a declining vegetation trend in the middle of 2005. This indicates a period of reforestation, as evidenced by an increase in vegetation in the middle of 2007, reaching a peak value similar to that of 2003 before the decline occurred. For P1 and P2, the major breakpoints occurred around 2013–2014, after which NDVI remained consistently low, suggesting land clearing and conversion. This timing aligns with the mapped urban expansion peak during 2010–2015, and with accelerated infrastructure-led development in Makassar during the mid-study period. The P3 illustrates that NDVI decline is not always monotonic: partial recovery may occur before a later breakpoint, reflecting temporary vegetation regrowth on undeveloped parcels prior to final conversion.

Seasonal variability in NDVI is expected, with higher values typically observed during the rainy season and lower values during the dry season. The CCDC harmonic model explicitly accounts for this seasonal behavior by fitting periodic terms to the NDVI time series and identifying breakpoints only when deviations are persistent and statistically significant, thereby reducing the risk of misinterpreting normal seasonal fluctuations as land cover change [29].

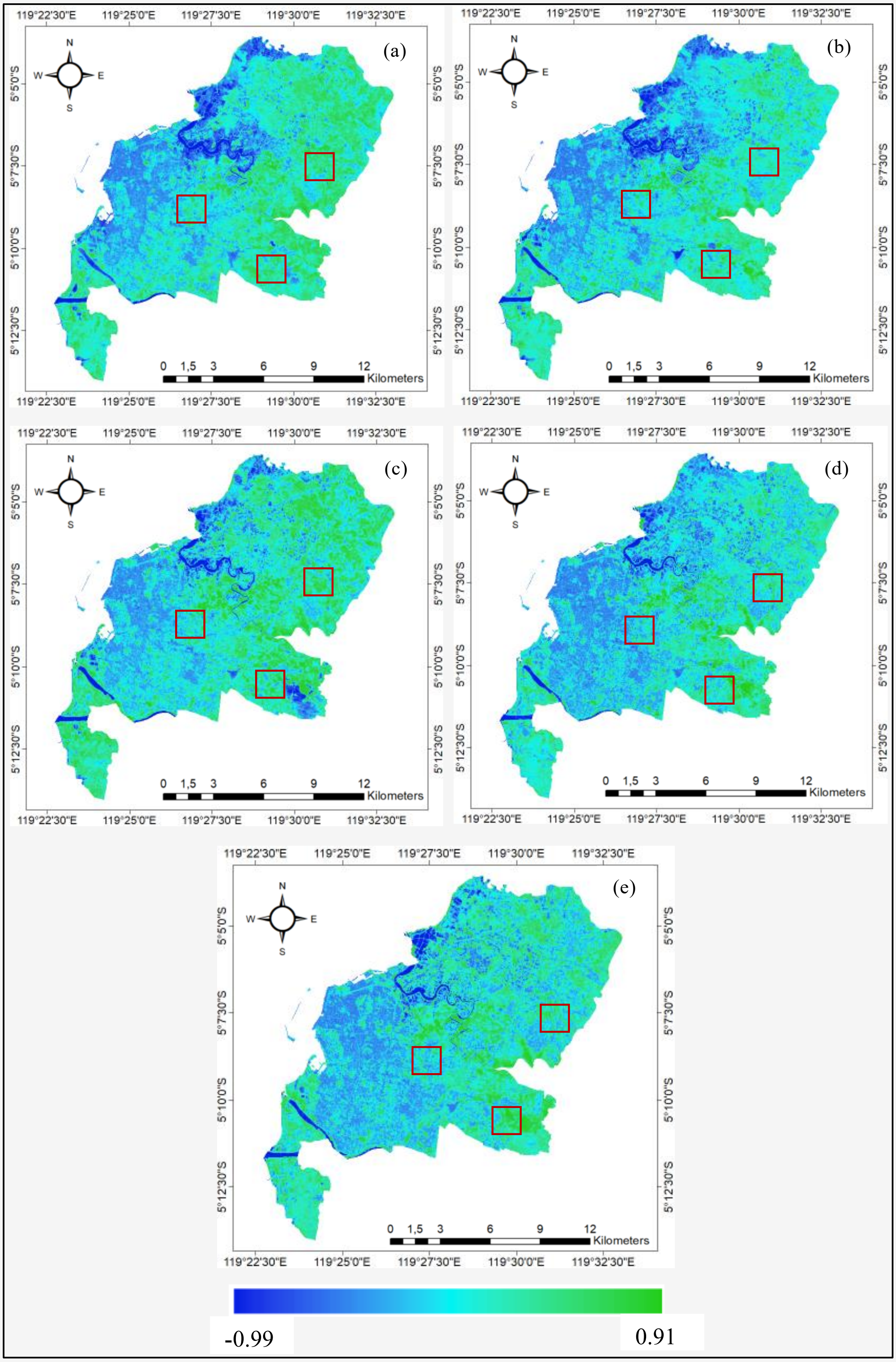

Figure 4: The distribution of NDVI in: (a) 2000; (b)2005; (c) 2010; (d) 2015; and (e) 2020

ISSN: 1686-6576 (Printed) | ISSN 2673-0014 (Online) | © Geoinformatics International

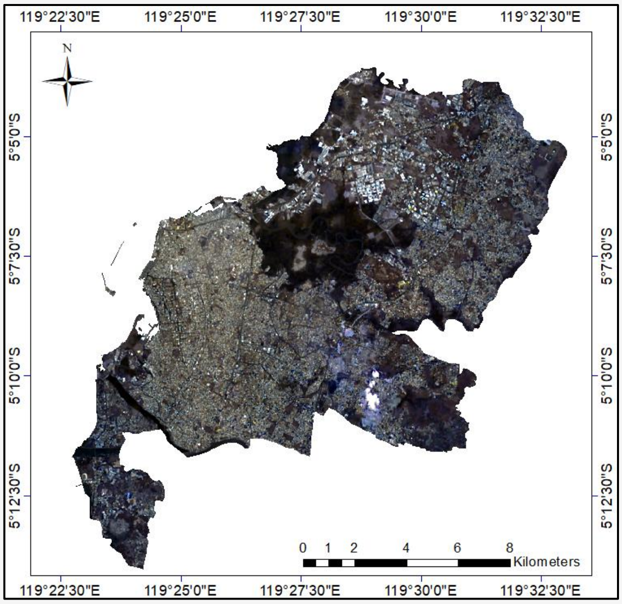

Figure 5: Points map of coordinates samples

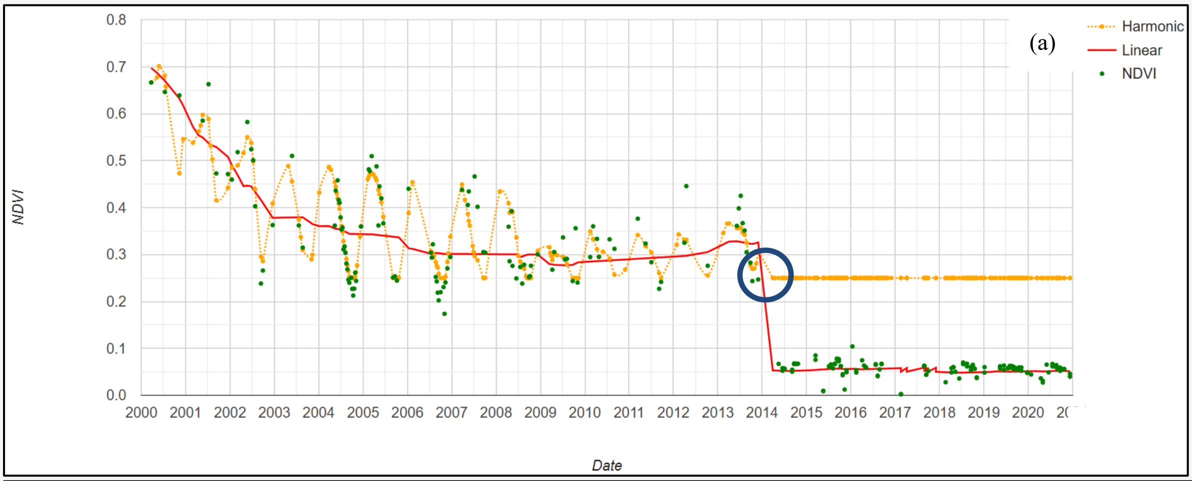

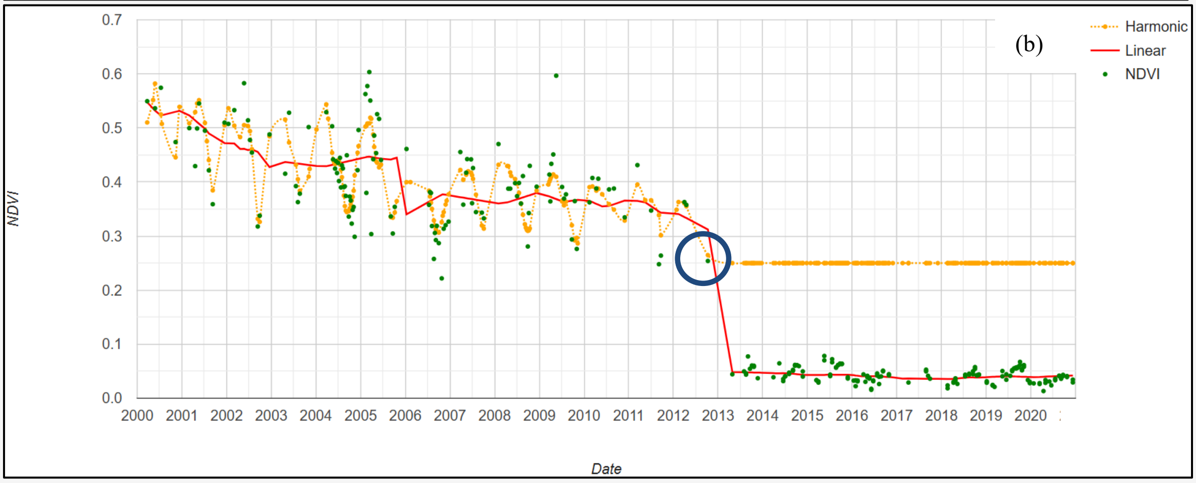

Figure 6: Harmonic approach for detection vegetation change trends: (a) p1, and (b) p2 (continue next page)

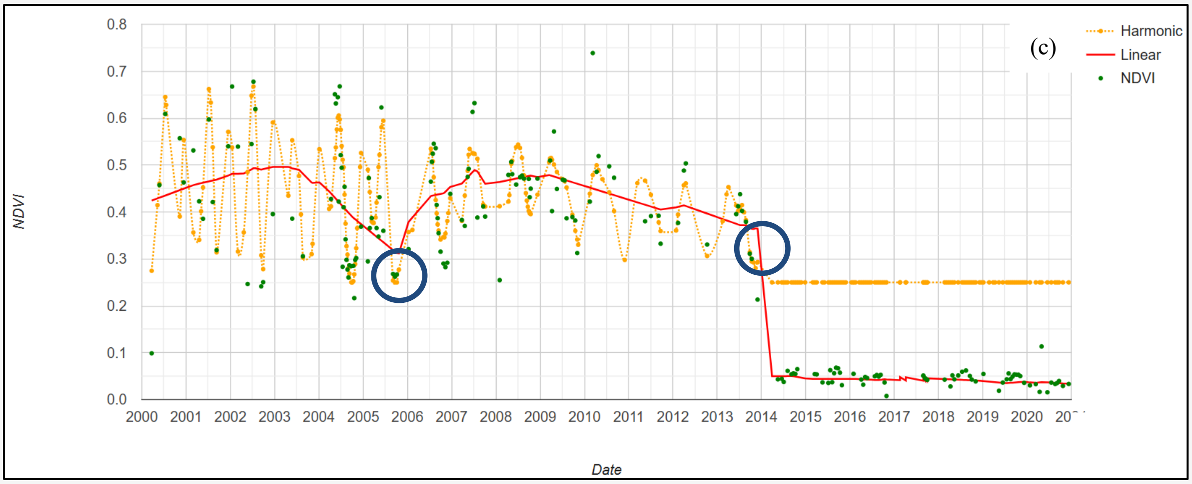

Figure 7: Harmonic approach for detection vegetation change trends: (a) p1, (b) p2, and (c) p3 (continue from previous page)

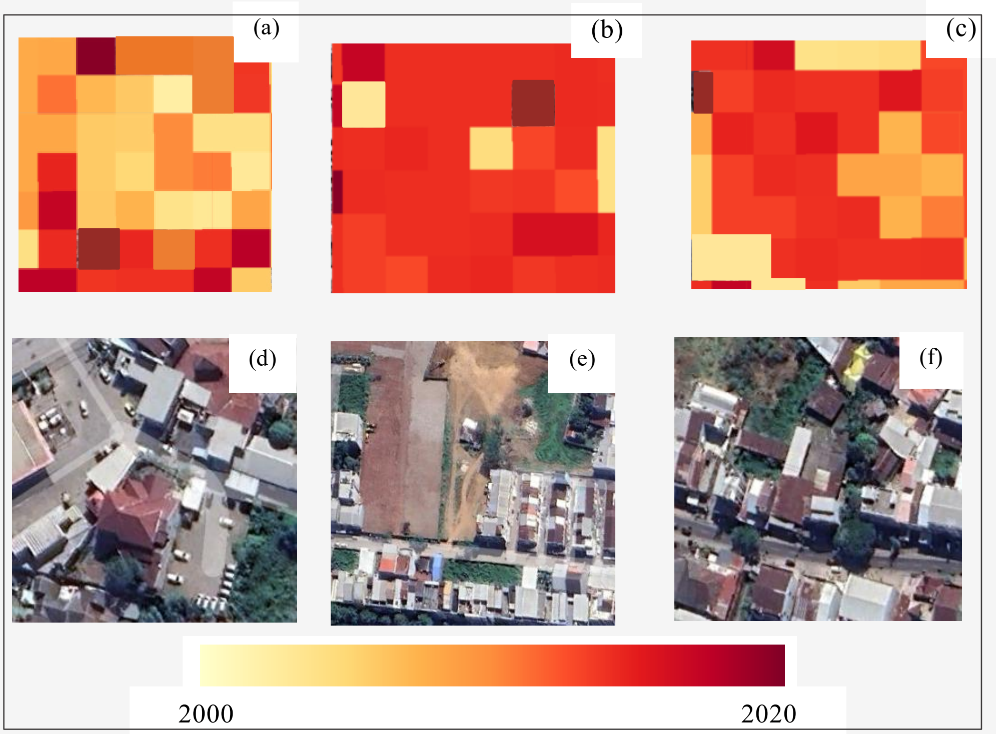

Figure 8: Vegetation pixel changed over time and location of observation: (a) pixel location P1, (b) pixel location P2, (c) pixel location P3, (d) image location P1, (e) image location P2, and (f) image location P3

Figure 7 shows that vegetation change detected by the model does not necessarily follow a monotonic decline; temporary recovery or stabilization may occur before a subsequent breakpoint. This capability allows the harmonic approach to distinguish gradual or staged vegetation conversion from short-term climatic effects, providing a more reliable interpretation of urban-induced vegetation change. Several vegetation breakpoints coincide with periods of rapid urban expansion and infrastructure development due to large-scale construction activities often require land clearing and vegetation removal.

Figure 8 illustrates areas of vegetation decline according to the year of change, based on pixel data representing a 10 × 10-meter area. The figure highlights the spatial progression of vegetation loss, with earlier changes occurring near established urban cores and more recent losses concentrated along northern and eastern peri-urban corridors. This pattern reflects staged land conversion associated with outward urban expansion rather than uniform

ISSN: 1686-6576 (Printed) | ISSN 2673-0014 (Online) | © Geoinformatics International

vegetation decline across the city. The validation results indicate a strong agreement between ground truth observations and Landsat-derived estimates, as reflected by the high coefficient of determination and relatively low error values. The regression analysis showed a strong linear relationship between the ground truth observations and the Landsat-derived estimates ($R^2 = 0.927$) with low prediction errors (RMSE = 0.042 and MAE = 0.034). These results indicate a high level of agreement between the two datasets and confirm the reliability of the satellite-derived estimates for representing ground conditions. These statistical metrics demonstrate that the Landsat-derived estimates provide a reliable representation of the observed conditions. The relationship between the datasets, including the regression line and validation statistics, is illustrated in Figure 9(a).

The residual distribution analysis was performed to evaluate the prediction errors of the Random Forest model. Residuals represent the difference between the predicted Landsat-derived values and the corresponding ground truth observations. As shown in Figure 9(b), most residual values are clustered around zero, indicating that the model predictions are generally close to the observed measurements. A relatively narrow residual range indicates that most prediction errors are small and centered near zero. This suggests that the model produces accurate and unbiased predictions, with limited deviation between the Landsat-derived estimates and the ground truth observations. The stable residual distribution also confirms the low RMSE and MAE values obtained during the validation process, supporting the reliability of the regression model.

3.3 LST Distribution in Urban Area

The distribution of surface temperature serves as one of the most tangible indicators of climate change. Based on the results of LST distribution mapping in Makassar City, the spatial pattern of LST showed clear intra-urban contrasts and inter-annual variability. To ensure that LST values were comparable between years, LST was summarized using annual composites generated from Landsat observations within a consistent seasonal window each year (Section 2.4). This approach reduces bias from wet–dry seasonal differences and allows inter-annual comparison of surface thermal conditions.

According to the LST calculation results, as illustrated in Figure 8, in the year 2000, the highest recorded pixel value was 42.16 °C, while pixel-level minimum values were excluded from interpretation due to potential residual cloud, water-body, and edge artefacts. Because pixel-level minimum/maximum values are sensitive to residual cloud contamination, water pixels, and edge artefacts, inter-annual comparison was based primarily on robust summary statistics (such as median LST and/or percentile ranges) rather than on extreme values. Furthermore, although global data indicate a consistent warming trend, climate fluctuations at local and regional scales can still be highly significant. Therefore, the average temperature in a specific city, province, or country does not always align directly with the global warming pattern but may vary according to natural climate dynamics and local environmental conditions. The fluctuations in LST may also be associated with vegetation dynamics observed during the study period. Areas experiencing vegetation loss tend to exhibit higher surface temperatures due to reduced evapotranspiration and increased heat absorption by impervious surfaces.

The increase in temperature can be observed through the median LST (the median value of all valid LST pixels within the study area) summarized at five-year intervals over two decades. While an overall warming trend is evident, the median LST values exhibit interannual fluctuations rather than a strictly consistent increase. In the year 2000, the median temperature was 22.21°C, which then increased to 27.29°C.

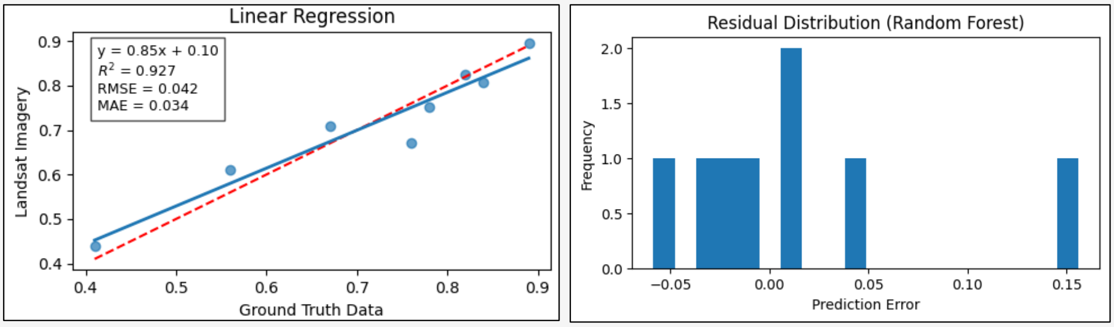

Figure 9: (a) Linear regression of Landsat and ground truth data, and (b) residual distribution

ISSN: 1686-6576 (Printed) | ISSN 2673-0014 (Online) |

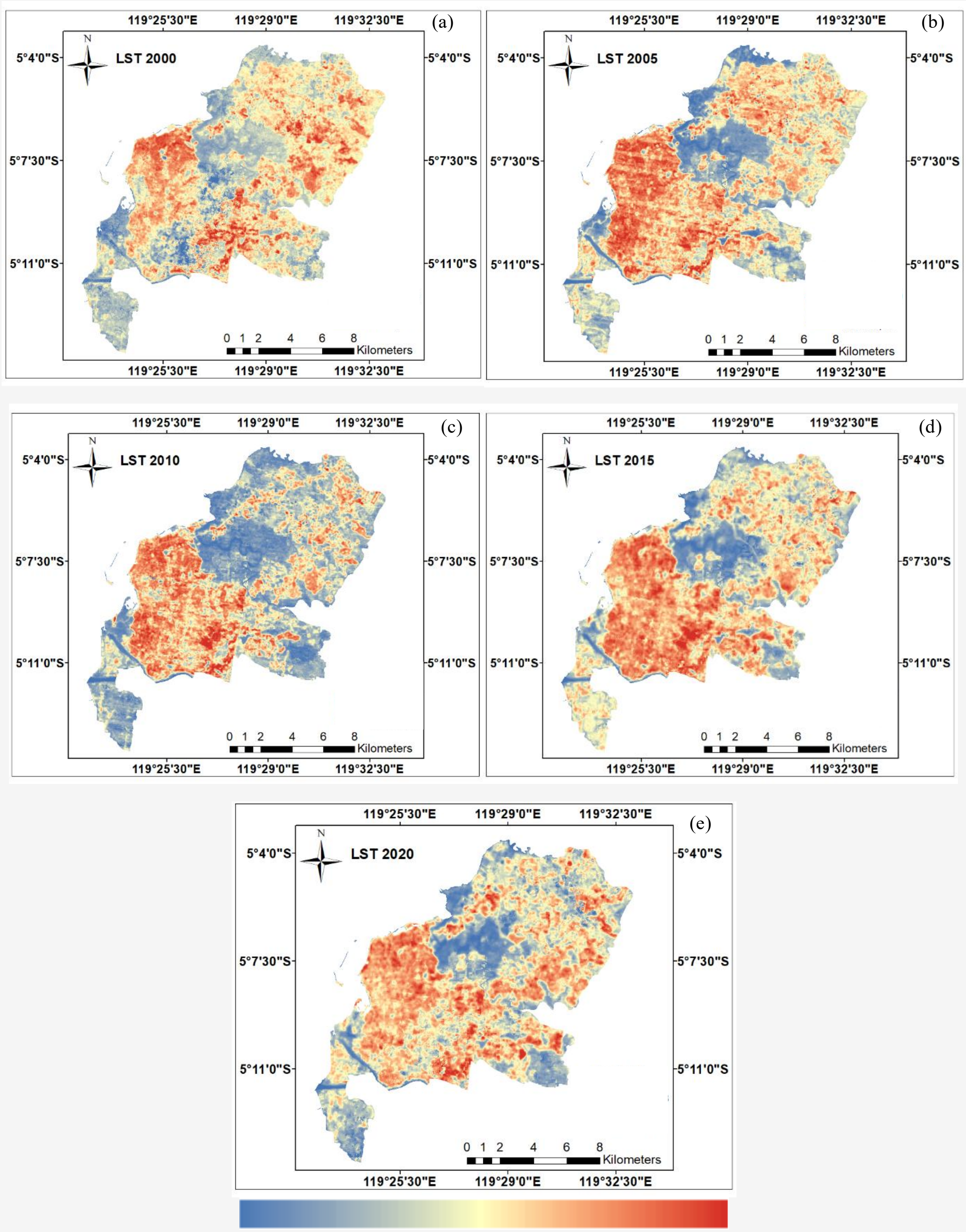

17.23°C 42.16°C

Figure 10: LST distribution in Makassar over the past two decades: (a) 2000, (b) 2005, (c) 2010, (d) 2015, and (e) 2020

Spatially, higher LST zones expanded from the established western or coastal urban core toward the central and northern–eastern growth corridors, consistent with the mapped pattern of built-up expansion (Section 3.1) and vegetation decline (Section 3.2). By 2010, the median surface temperature had increased to 28.04°C, followed by a gradual rise in 2015, reaching 29.64°C, representing the highest recorded average temperature. This temperature increase expanded from the western region to the central part of the study area, as shown in Figure 10. In 2020, the final year of observation, the average temperature slightly declined from the previous year, reaching 28.16°C. These findings indicate that localized LST hotspots in Makassar are closely associated with urban morphology and land-use intensity, particularly in dense built-up zones and transportation-dominated areas.

Based on the median LST values, surface thermal conditions increased overall over the past two decades. Areas experiencing vegetation loss generally exhibited higher LST, consistent with the spatial patterns observed in Sections 3.1 and 3.2. Figure 11 illustrates that the slope of the median LST time series was 0.285 °C per year, indicating a gradual warming trend over the study period. This relationship is particularly evident from the vegetation changes that occurred in 2013–2014. Furthermore, during the field survey, temperature variations were measured alongside vegetation assessments, revealing that sampling points with reduced vegetation tended to exhibit higher temperatures. This R^2 value indicates a moderate temporal trend, suggesting that while time explains a substantial portion of LST variability, other factors such as land-cover change and inter-annual climate variability also play important roles. The R^2 value of 0.63 indicates a moderate yet statistically meaningful temporal trend in LST. Although the mean values demonstrate a consistent long-term increase, seasonal variability is present in [28] and short-term declines in specific years reduce the strength of the linear relationship, resulting in a moderate R-square. This reflects the inherently non-linear behaviour of urban thermal dynamics.

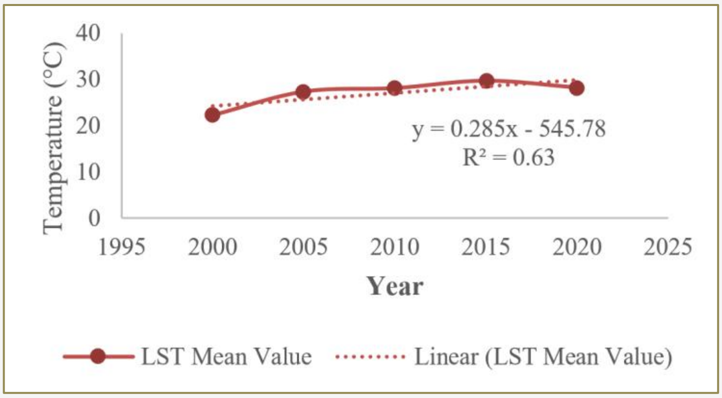

Figure 11: LST mean value

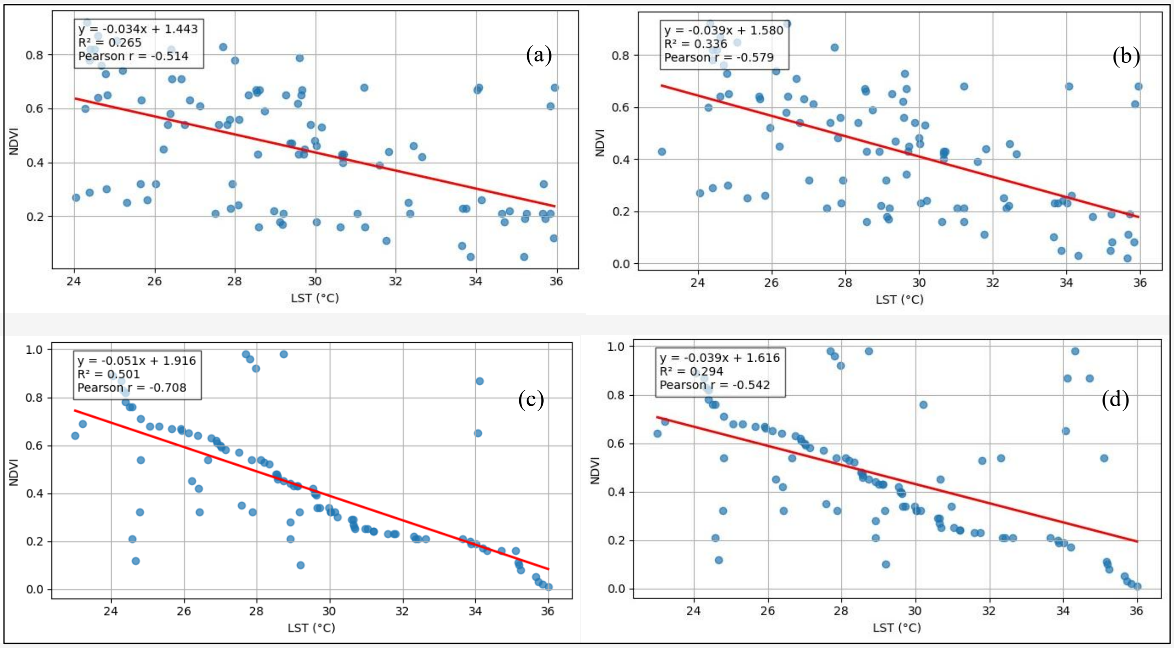

Figure 12: Pearson's correlation between LST and NDVI: (a) 2005, (b) 2010, (c) 2015, and (d) 2020

ISSN: 1686-6576 (Printed) | ISSN 2673-0014 (Online) |

Overall, the findings suggest that both progressive urbanization and interannual climate variability shape LST patterns over time. To further quantify the relationship between vegetation cover and surface temperature, a scatter plot analysis between LST and NDVI was conducted for 2005, 2010, 2015, and 2020. The results in Figure 12 indicate a consistent negative relationship, with Pearson correlation coefficients ranging from −0.514 to −0.708, suggesting that areas with higher vegetation density generally exhibit lower surface temperatures. The strongest correlation was observed in 2015 ($r = -0.708$, $R^2 = 0.501$), indicating that vegetation cover played a stronger role in moderating surface temperature during that period. These results quantitatively support the spatial observations, confirming that reductions in vegetation cover are associated with increased LST in the study area.

4. Conclusion

The results show that Makassar experienced substantial land-cover transformation between 2000 and 2020, with the most rapid expansion of built-up areas occurring during 2010–2015, when several areas exhibited a marked decline in vegetation, with NDVI values decreasing to around 0.2. This expansion corresponded with vegetation loss and the emergence of localized SUHI hotspots, particularly as urban growth shifted from the coastal core toward the northern and eastern peri-urban corridors. Using a harmonic time-series approach, CCDC successfully detected statistically significant NDVI breakpoints around 2013–2014, aligning with the period of accelerated urban development and demonstrating its effectiveness for monitoring rapid land-cover change in tropical urban environments. Although NDVI decline indicates vegetation loss, it does not independently confirm specific land-cover transitions; therefore, the interpretation was supported by urban sprawl extraction results and visual verification using high-resolution imagery. Future studies should incorporate explicit LULC transition mapping and accuracy assessment to strengthen attribution. From a practical perspective, the findings highlight priority mitigation zones in Makassar, particularly along rapidly developing northern and eastern corridors, where strengthening urban green infrastructure such as green belts, street trees, and protected peri-urban vegetation could help reduce SUHI intensity. Overall, this study demonstrates the value of CCDC-based harmonic time-series analysis as a robust framework for long-term monitoring of vegetation change and urban heat dynamics in cloud-prone tropical cities.

Acknowledgment

We sincerely extend our deepest gratitude to Lembaga Penelitian dan Pengabdian Masyarakat (LPPM) Universitas Hasanuddin, for their unwavering support and the generous research grant, Grant Number 01260/UN4.22/PT.01.03/2025, which made this research feasible.

References

[1] Maurer, J. M., Schaefer, J., Rupper, S. and Corley, A., (2019). Acceleration of Ice Loss Across the Himalayas Over the Past 40 Years. *Science Advances*, Vol. 5(6). https://doi.org/10.1126/sciadv.aav7266.

[2] Solomon, S., (2007). *Climate Change 2007: The Physical Science Basis: Working Group I Contribution to the Fourth Assessment Report of the IPCC*. Cambridge University Press.

[3] Jaswal, S. and Thakur, P., (2023). Correlation Between LST, NDVI And NDBI With Reference to Urban Sprawling: A Case Study of Shimla City. *International Journal of Multidisciplinary Research*, Vol. 5; 1-14. https://doi.org/10.36948/ijfmr.2023.v05i06.10258.

[4] Zhang, Y., Odeh, I. O. and Han, C., (2009). Bi-Temporal Characterization of Land Surface Temperature in Relation to Impervious Surface Area, NDVI and NDBI, Using a Sub-Pixel Image Analysis. *International Journal of Applied Earth Observation and Geoinformation*, Vol. 11(4); 256-264. https://doi.org/10.1016/j.jag.2009.03.001.

[5] Surya, B., Salim, A., Hernita, H., Suriani, S., Menne, F. and Rasyidi, E. S., (2021). Land Use Change, Urban Agglomeration, and Urban Sprawl: A Sustainable Development Perspective of Makassar City, Indonesia. *Land*, Vol. 10(6). https://doi.org/10.3390/land10060556.

[6] Alexander, C., (2020). Normalised Difference Spectral Indices and Urban Land Cover as Indicators of Land Surface Temperature (LST). *International Journal of Applied Earth Observation and Geoinformation*, Vol. 86. https://doi.org/10.1016/j.jag.2019.102013.

[7] Nurwanda, A. and Honjo, T., (2018). Analysis of Land Use Change and Expansion of Surface Urban Heat Island in Bogor City by Remote Sensing. *ISPRS International Journal of Geo-Information*, Vol. 7(5); 165. https://doi.org/10.3390/ijgi7050165.

[8] Tran, D. X., Pla, F., Latorre-Carmona, P., Myint, S. W., Caetano, M. and Kieu, H. V., (2017). Characterizing the Relationship between Land Use Land Cover Change and Land Surface Temperature. *ISPRS Journal of Photogrammetry and Remote Sensing*, Vol. 124; 119-132. https://doi.org/10.1016/j.isprsjprs.2017.01.001.

[9] Quattrochi, D. A. and Luvall, J. C., (1999). Thermal Infrared Remote Sensing for Analysis of Landscape Ecological Processes: Methods and Applications. *Landscape Ecology*. Vol. 14; 577-598. https://doi.org/10.1023/A:1008168910634.

[10] Ramli, I., Achmad, A., Nizamuddin, N., Izzaty, A. and Irzaidi, I., (2023). Transformation of Land Use and Land Cover and Its Implication to the Local Climate in Aceh Besar District, Aceh, Indonesia. *IOP Conference Series: Earth and Environmental Science*, https://doi.org/10.1088/1755-1315/1263/1/012023.

[11] Aldileemi, H., Zhran, M., and El-Mewafi, M. (2023). Geospatial Monitoring and Prediction of land Use/Land Cover (LULC) Dynamics Based on the CA-Markov Simulation Model in Ajdabiya, Libya. *International Journal of Geoinformatics*, Vol. 19(12), 15–29. https://doi.org/10.52939/ijg.v19i12.2973.

[12] Choudhury, D., Das, K. and Das, A., (2019). Assessment of Land Use Land Cover Changes and Its Impact on Variations of Land Surface Temperature in Asansol-Durgapur Development Region. *The Egyptian Journal of Remote Sensing and Space Science*. Vol. 22(2); 203-218. https://doi.org/10.1016/j.ejrs.2018.05.004.

[13] Thammaboribal, P. (2024). Investigating Land Surface Temperature Variation and Land Use Land Cover Changes in Pathumthani, Thailand (1997-2023) using Landsat Satellite Imagery: A Comprehensive Analysis of LST and Urban Hot Spots (UHS). *International Journal of Geoinformatics*, Vol. 20(2); 27–41. https://doi.org/10.52939/ijg.v20i2.3063.

[14] Arshad, S., Ahmad, S. R., Abbas, S., Asharf, A., Siddiqui, N. A. and ul Islam, Z., (2022). Quantifying the Contribution of Diminishing Green Spaces and Urban Sprawl to Urban Heat Island Effect in a Rapidly Urbanizing Metropolitan City of Pakistan. *Land Use Policy*, Vol. 113. https://doi.org/10.1016/j.landusepol.2021.105874.

[15] Rahimi, E., Dong, P. and Jung, C., (2025). Global NDVI-LST Correlation: Temporal and Spatial Patterns from 2000 to 2024. *Environments*, Vol. 12(2). https://doi.org/10.3390/environments12020067.

[16] Sun, D. and Kafatos, M., (2007). Note On the NDVI-LST Relationship and the Use of Temperature-Related Drought Indices over North America. *Geophysical Research Letters*, Vol. 34(24). https://doi.org/10.1029/2007GL031485.

[17] Grover, A. and Singh, R. B., (2015). Analysis of Urban Heat Island (UHI) in Relation to Normalized Difference Vegetation Index (NDVI): A Comparative Study of Delhi and Mumbai. *Environments*, Vol. 2(2); 125-138. https://doi.org/10.3390/environments2020125.

[18] Jagtap, A., Shedge, D., and Mane, P. (2024). Exploring the Effects of Land Use/Land Cover (LULC) Modifications and Land Surface Temperature (LST) in Pune, Maharashtra with Anticipated LULC for 2030. *International Journal of Geoinformatics*, Vol. 20(2), 42–63. https://doi.org/10.52939/ijg.v20i2.3065.

[19] Zhu, Z. and Woodcock, C. E., (2014). Continuous Change Detection and Classification of Land Cover Using all Available Landsat Data. *Remote Sensing of Environment*, Vol. 144; 152-171. https://doi.org/10.1016/j.rse.2014.01.011.

[20] Izzaty, A. and Sukojo, B. M., (2021). Identification of Land Criticality with the Application of Deep Learning in West Lahat District using Sentinel-2A Imagery. *IOP Conference Series: Earth and Environmental Science*. https://doi.org/10.1088/1755-1315/936/1/012009.

[21] Izzaty, A., Ramli, I. and Bakri, B., (2026). Water Quality Estimation from Total Suspended Solid and Dissolved Oxygen Concentration in Krueng Pase Watershed, North Aceh, Indonesia. *International Journal of Environmental Impacts*, Vol. 9(1); 62-73. https://doi.org/10.56578/ijei090106.

[22] Gómez-Chova, L., Amorós-López, J., Mateo-García, G., Muñoz-Marí, J. and Camps-Valls, G., (2017). Cloud Masking and Removal in Remote Sensing Image Time Series. *Journal of Applied Remote Sensing*, Vol. 11(1). https://doi.org/10.1117/1.JRS.11.015005.

[23] Candra, D., Phinn, S. and Scarth, P., (2016). Cloud and Cloud Shadow Masking Using Multi-Temporal Cloud Masking Algorithm in Tropical Environmental. *The International Archives of the Photogrammetry, Remote Sensing and Spatial Information Sciences*, Vol. XLI-B2; 95-100. https://doi.org/10.5194/isprs-archives-XLI-B2-95-2016.

[24] Zhu, Z., Woodcock, C. E. and Olofsson, P., (2012). Continuous Monitoring of Forest Disturbance Using all Available Landsat Imagery. *Remote Sensing of Environment*, Vol. 122; 75-91. https://doi.org/10.1016/j.rse.2011.10.030.

[25] Ramadhan, F. D., Hariyanto, T. and Handayani, H. H., (2021). Analysis of Urban Built-Up Expansion Based on Combination of Spectral Indices in Surabaya City. *Geoid*, Vol. 17(1); 21-37. https://doi.org/10.12962/j24423998.v17i1.8676.

[26] Sobrino, J. A., Jiménez-Muñoz, J. C. and Paolini, L., (2004). Land Surface Temperature Retrieval from LANDSAT TM 5. *Remote Sensing of Environment*, Vol. 90(4); 434-440. https://doi.org/10.1016/j.rse.2004.02.003.

[27] Sobrino, J. A., Jiménez-Muñoz, J. C., Sòria, G., Romaguera, M., Guanter, L. and Moreno, J., (2008). Land Surface Emissivity Retrieval from Different VNIR and TIR Sensors. *IEEE Transactions on Geoscience and Remote Sensing*, Vol. 46(2); 316-327. https://doi.org/10.1109/TGRS.2007.904834.

[28] Mumtaz, F., Tao, Y., De Leeuw, G., Zhao, L., Fan, C. and Elnashar, A., (2020). Modeling Spatio-Temporal Land Transformation and Its Associated Impacts on Land Surface Temperature (LST). *Remote Sensing*, Vol. 12(18). https://doi.org/10.3390/rs12182987.

[29] Ayanlade, A., Jeje, O. D., Nwaezeigwe, J. O., Orimoogunje, O. O. and Olokeogun, O. S., (2021). Rainfall Seasonality Effects on Vegetation Greenness in Different Ecological Zones. *Environmental Challenges*. Vol. 4. https://doi.org/10.1016/j.envc.2021.100144.